JACS
JOURNAL OF THE AMERICAN CHEMICAL SOCIETY
Communication
pubs.acs.org/JACS

Bifacial DNA Origami-Directed Discrete, Three-Dimensional, Anisotropic Plasmonic Nanoarchitectures with Tailored Optical Chirality

Xiang Lan,† Zhong Chen,† Gaole Dai, Xuxing Lu, Weihai Ni, and Qiangbin Wang*

Suzhou Key Laboratory of Nanobiomedical Characterization, Division of Nanobiomedicine and *i*-Lab, Suzhou Institute of Nano-Tech and Nano-Bionics, Chinese Academy of Sciences, Suzhou 215123, China

Supporting Information

ABSTRACT: Discrete three-dimensional (3D) plasmonic nanoarchitectures with well-defined spatial configuration and geometry have aroused increasing interest, as new optical properties may originate from plasmon resonance coupling within the nanoarchitectures. Although spherical building blocks have been successfully employed in constructing 3D plasmonic nanoarchitectures because their isotropic nature facilitates unoriented localization, it still remains challenging to assemble anisotropic building blocks into discrete and rationally tailored 3D plasmonic nanoarchitectures. Here we report the first example of discrete 3D anisotropic gold nanorod (AuNR) dimer nanoarchitectures formed using bifacial DNA origami as a template, in which the 3D spatial configuration is precisely tuned by rationally shifting the location of AuNRs on the origami template. A distinct plasmonic chiral response was experimentally observed from the discrete 3D AuNR dimer nanoarchitectures and appeared in a spatial-configuration-dependent manner. This study represents great progress in the fabrication of 3D plasmonic nanoarchitectures with tailored optical chirality.

Well-defined plasmonic nanoarchitectures are of great significance in the study of plasmon-enhanced single-molecule spectroscopy,[1,2] plasmonic chiral optics,[3,4] nanophotonic[5,6] and nanoelectronic devices,[7] etc. A variety of one-dimensional (1D) and two-dimensional (2D) plasmonic nanostructures have been achieved, and organic polymers,[8] DNA motifs,[9,10] and monofacial 2D DNA origami with capturing strands extending from one side[11−13] have been widely used as templates. However, 3D plasmonic nanoarchitectures with precise control of particle size, interparticle distance, and geometric configuration may exhibit novel optical, electronic, and magnetic properties,[14−16] which are rarely realized in 1D and 2D nanostructures. In particular, rational organization of anisotropic metallic building blocks in 3D space may result in plasmonic chiral optical properties, which have been studied theoretically, for instance, in plasmonic nanorod assemblies.[17,18] To date, in bottom-up construction of 3D plasmonic nanoarchitectures, spherical nanoparticles are mostly used because their isotropic nature facilitates unoriented localization.[4,19,20] In the case of 3D nanoarchitectures composed of anisotropic building blocks, only examples of gold nanorod (AuNR) supra-aggregates lacking precise spatial control have been reported.[21,22] Directed assembly of anisotropic metallic building blocks into discrete and tailored 3D plasmonic nanoarchitectures still remains challenging. Unlike spherical metallic nanoparticle assemblies, for which the understanding of plasmonic chirality on the basis of plasmon hybridization theory is well-established,[3,4] examples of discrete 3D anisotropic building block nanoarchitectures displaying chiral optical activity are scarce.

Bifacial DNA origami, a facile template in which capturing strands protrude from opposite sides of a 2D DNA origami,[7,23] enables the construction of plasmonic nanoarchitectures in 3D space by directing the self-assembly of metallic building blocks on both sides. Meanwhile, the original large dimension of such a 2D bifacial template is preserved as compared with DNA helix bundles[3] and rolled origami tubes,[4] which is advantageous for assembling large anisotropic building blocks. However, the unique 3D addressability of bifacial DNA origami is still far from being fully exploited. Herein we demonstrate the ability of a bifacial DNA origami scaffold to precisely organize anisotropic AuNRs in 3D space. The first example of discrete 3D AuNR dimers with controlled interparticle distance and spatial orientation was obtained by precisely assembling the AuNRs on opposite sides of a rectangular bifacial DNA origami. Tuning the docking position of the AuNRs allowed the 3D spatial configuration of the obtained plasmonic nanoarchitectures to be manipulated well. The optical properties of the assembled nanoarchitectures were characterized using circular dichroism (CD) spectroscopy. For the first time, we experimentally observed the chiral optical response of the discrete 3D AuNR dimer nanoarchitectures. Furthermore, the resultant optical chirality was rationally tailored by modifying the 3D spatial configuration and geometric symmetry of the AuNR dimer nanoarchitectures.

As illustrated in Figure 1, we employed a rectangular bifacial DNA origami (90 nm × 60 nm × 2 nm) that was self-assembled from a long single-stranded (ss) M13 viral genomic DNA folded by a set of ∼200 short staple strands through sequence-specific hybridization and formation of multiples of DNA crossover, according to a reported method with some modifications.[24] Two types of capturing strands (shown in green and red) were rationally designed on opposite sides of the 2D bifacial DNA origami by extending 15 nucleotides from

Received: May 1, 2013
Published: July 23, 2013

   dx.doi.org/10.1021/ja404354c | *J. Am. Chem. Soc.* 2013, 135, 11441−11444

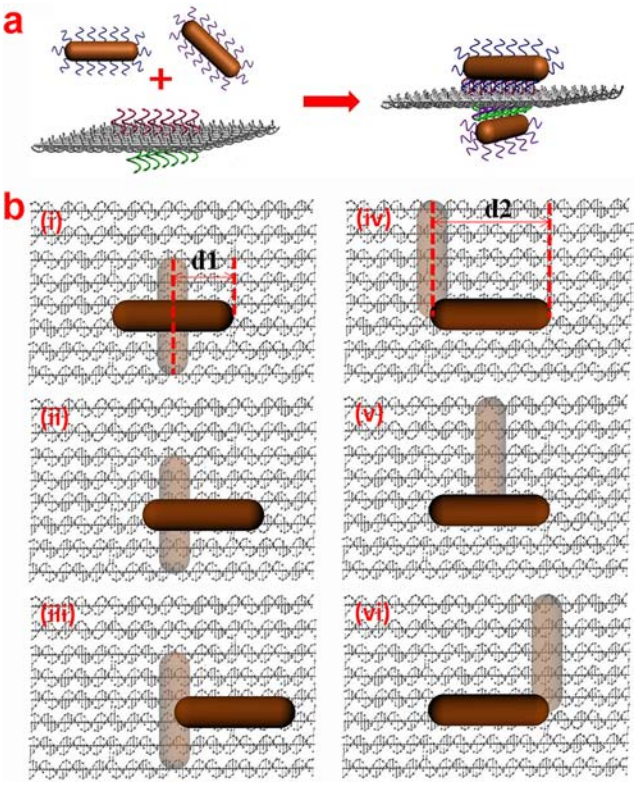

Figure 1. Scheme of the bifacial DNA origami-directed self-assembly of 3D AuNR dimer nanoarchitectures. (a) ssDNA-modified AuNRs (11 nm × 37 nm) were assembled on opposite sides of a 2D rectangular bifacial DNA origami template, generating discrete 3D AuNR dimer nanoarchitectures. Two sets of seven capturing strands (shown in red and green) were designed to localize a single AuNR on each side of the origami using hybridization-based rules. The seven capturing strands were optimized to have a width of ~37 nm, matching well with the size of AuNRs. (b) A series of 3D AuNR dimer nanoarchitectures was assembled by precisely shifting the location of the capturing strands on the origami template: (i) X1 (d_1 = 18.5 nm); (ii) X2 (d_1 = 28 nm); (iii) T1 (d_1 = 37 nm); (iv) L1 (d_2 = 37 nm); (v) T2 (d_2 = 18.5 nm); (vi) L2 (d_2 = 0 nm). Thus, the spatial configuration of these 3D nanoarchitectures was successfully tuned.

selected staple strands. Seven copies of DNA sticky ends were used to precisely dock a single AuNR at the predesigned location on each side of the bifacial DNA origami [see the Supporting Information (SI) for details]. The interparticle distance was defined to be 12 nm, taking account of the molecule length of two batches of capturing strands and the thickness of the origami template. Previous theoretical studies have shown that the configuration and geometric symmetry of the 3D plasmonic nanoarchitecture strongly affect the plasmon coupling within the nanoarchitecture and the resultant chiral optical activity.[17,18] Therefore, to precisely tailor the plasmonic chirality of the discrete 3D AuNR dimer nanoarchitectures, we rationally tuned the locations of the AuNRs on the origami template at nanometer scale by varying d_1 from 18.5 to 28 to 37 nm and d_2 from 37 to 18.5 to 0 nm. As a result, AuNRs were localized on opposite sides of the bifacial DNA origami in predefined patterns, generating 3D AuNR dimers with precisely tailored spatial configurations and geometric symmetries.

Figure 2a,b shows agarose gel images (stained with SYBR Green) of the AuNR dimer nanoarchitectures assembled on the bifacial DNA origami under daylight and UV light, respectively. The bands are sharp without smearing, indicating their good

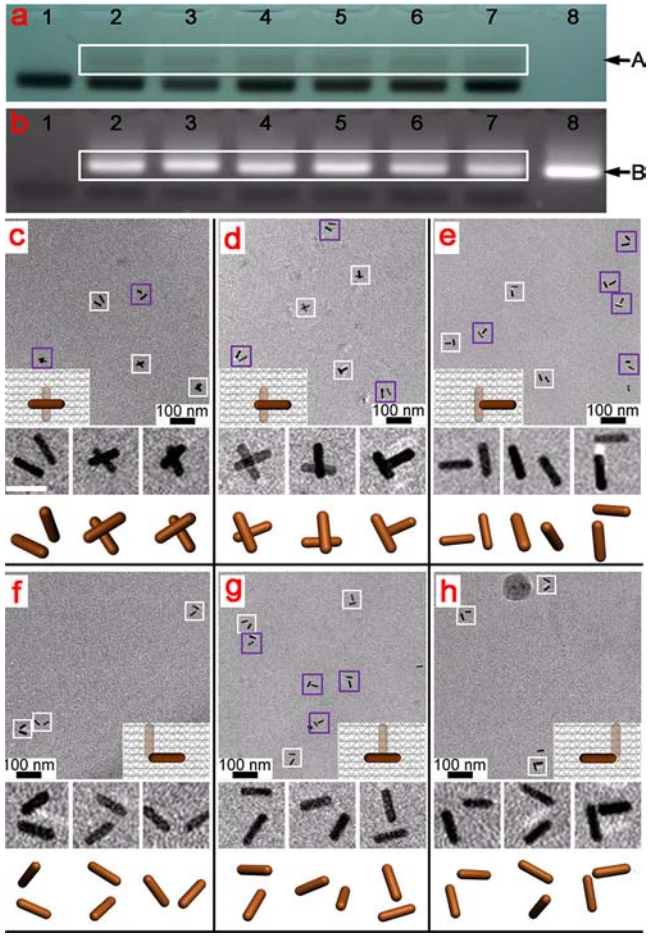

Figure 2. Characterization of the as-obtained 3D AuNR dimer nanoarchitectures. (a, b) SYBR Green-stained agarose gels of the AuNR dimer nanoarchitectures assembled on the bifacial DNA origami taken under (a) daylight and (b) UV light. Lane 1, 11 nm × 37 nm AuNRs. Lanes 2–7: AuNR dimers X1, X2, T1, L1, T2, and L2, respectively. Lane 8: purified rectangular bifacial origami. (c–h) Cryo-EM images of 3D AuNR dimer nanoarchitectures assembled on bifacial DNA origami (top row), close-up views of white-boxed structures (middle row), and corresponding model structures with specific orientations (bottom row): (c) X1; (d) X2; (e) T1; (f) L1; (g) T2; (h) L2. The scale bar in the high magnification image is 40 nm. The observed structures are in good agreement with the designed model structures, proving the validity of our strategy. The 3D AuNR dimer nanoarchitectures labeled in purple were reconstructed and are presented in Figure S3.

monodispersity. Lanes 2–7 in band A contained AuNR dimers X1, X2, T1, L1, T2, and L2, respectively. All of these nanoarchitectures assembled on the bifacial DNA origami exhibited approximately the same mobility as the underlying origami template because of the much larger size of the origami. As shown in Figure 2b, band B of the pure DNA origami (lane 8) and the directed assemblies (lanes 2–7) moved at similar speeds. The assembled plasmonic nanoarchitectures were purified and frozen in the ice layer for cryogenic electron microscopy (cryo-EM) imaging. The native geometries of the AuNR dimer nanoarchitectures were preserved, thus allowing for in situ 3D conformation identification and avoiding structural deformation resulting from conventional TEM sampling.

The top rows in Figure 2c–h present cryo-EM images of the obtained 3D AuNR dimer nanoarchitectures. It must be noted

dx.doi.org/10.1021/ja404354c | J. Am. Chem. Soc. 2013, 135, 11441–11444

that because of the different projection angles between the electron beam and the samples randomly oriented in the ice, various 2D projections of AuNR dimer nanoarchitectures were observed. We reconstructed the 3D AuNR dimer nanoarchitectures by rotating the 3D models with the same spatial parameters as designed (11 nm × 37 nm AuNRs with an interparticle distance of 12 nm). The close-up views of the AuNR dimer nanoarchitectures fit very well with the 3D model structures having the corresponding orientations (middle and bottom rows in Figure 2c–h). The high fidelity between the cryo-EM images and the models confirmed that the experimental observations truly were the designed nanoarchitectures. The low-magnification cryo-EM images reveal the high purity (>85%) of the obtained AuNR dimer nanoarchitectures, validating the subsequent plasmonic chirality measurements on the ensembles. The additional cryo-EM images and model structures presented in Figures S1–S3 in the SI further demonstrate the realization of the precise template-directed 3D arrangement of AuNRs on the bifacial DNA origami.

It has been demonstrated theoretically that plasmonic chiral response may occur from the 3D AuNR assemblies at the plasmon resonance frequency and exhibit a spatial-configuration-dependent character.[17] In the present study, the dimers X1, X2, T1, and T2 possess symmetric 3D spatial configurations, whereas L1 and L2 have asymmetric 3D configurations and act as a pair of mirror-symmetric structures resembling enantiomers in organic chemistry. The optical responses of the discrete 3D AuNR dimer nanoarchitectures were experimentally characterized using CD spectroscopy. Obviously, the CD spectra of the assembled 3D AuNR dimer nanoarchitectures (Figure 3) exhibit characteristic bisignate signatures with intensities much stronger than that of a single AuNR. Through modification of the plasmon coupling by shifting the location of one AuNR, a gradual decrease in the measured CD intensity in going from X1 to T1 was observed (Figure 3a). T2 had plasmonic chirality as weak as that of T1 because of its similar structure (Figure 3b). L1 and L2 exhibited the anticipated vertically mirrored CD signals, behaving as a pair of enantiomers. Thus, the chiroptical activity was significantly modulated by rational design of the geometry and spatial arrangement of the assembled 3D AuNR nanoarchitectures. For the symmetric nanoarchitectures (X1, T1, X2, and T2), a previous theoretical study reported that the orthogonally arranged AuNR dimer without a chiral molecule in close proximity exhibits no chiral response.[17] This suggests that the DNA origami plays a critical role in the plasmonic CD of the obtained AuNR dimer nanoarchitectures. Tang and co-workers reported that plasmon resonance coupling within AuNR supra-aggregates can enhance the chiral optical response of chiral double-stranded DNA serving as molecule glue.[21] More recently, Govorov and co-workers showed that a CD signal can be induced from chiral molecules at surface plasmon resonances of an achiral gold nanostructure when the chiral molecules are in proximity to the surface of the gold nanostructure.[25] Here, the DNA origami is thought to contribute to the chiral optical response of the symmetric nanoarchitectures of X1, T1, X2, and T2 through chirality transfer from the chiral DNA molecules to the surface plasmon of the AuNRs via a dipole–plasmon Coulomb interaction. This is quite similar to the situation of induction of chiroptical activity of biomolecules at the surface plasmon of achiral gold nanoislands.[25] Regarding the asymmetric nanoarchitectures that have a chiral arrangement (L1 and L2), the physical nature becomes complicated because both the chiral DNA–plasmon and plasmon–plasmon interactions contribute to the chiroptical activity. In a previous study on chiral molecule–chiral plasmonic nanostructures, the theoretical calculation was solely focused on the plasmon–plasmon interaction and disregarded the chiral molecule–plasmon interaction.[3] In this work, the mirror-symmetric configurations of L1 and L2 reversed the handedness of the resultant plasmonic CD spectra, clearly demonstrating the dominant role of the plasmon–plasmon interaction associated with the chiral geometry in determining the optical chirality.

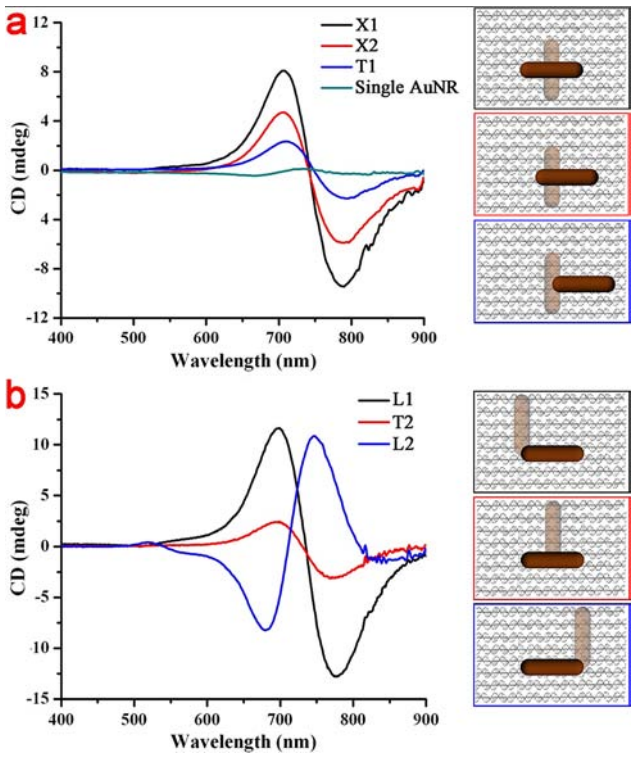

Figure 3. CD spectra of the discrete 3D plasmonic AuNR dimer nanoarchitectures: (a) X1, X2, and T1; (b) L1, T2, and L2. The concentrations of all of the samples were the same.

To obtain a deeper understanding of the plasmonic chirality of the obtained 3D AuNR dimers, we performed theoretical calculations on the pure metallic AuNR dimer nanoarchitectures without the DNA origami scaffold using the discrete dipole approximation (DDA) method to reveal their instinctive plasmonic characteristics. The models of the AuNR dimer nanoarchitectures used in the DDA calculations are shown in Figure S6. As illustrated in Figure S7, the symmetric metallic nanoarchitectures (X1, X2, T1, and T2) exhibit no chiral response, and the asymmetric metallic nanoarchitectures (L1 and L2) display significant chiroptical activity. For the symmetric metallic nanoarchitectures without DNA origami, the nonchiral response is attributed to their structural symmetry, which leads to the same absorbance of left-handed and right-handed circularly polarized light. These theoretical results are diametrically opposed to the experimental observations in Figure 3a. Thus, we expect that the experimentally observed plasmonic CD of the symmetric AuNR dimer nanoarchitectures originates from the DNA constituents excluded in the theoretical model, which involve

dx.doi.org/10.1021/ja404354c | J. Am. Chem. Soc. 2013, 135, 11441–11444

the intrinsic molecular chirality of the DNA origami as well as the flexibility of the DNA capturing strands and origami template, which may cause slight structural perturbations of the 3D AuNR dimer nanoarchitectures. On the contrary, the theoretical models of the asymmetric nanoarchitectures exhibit notable reversed CD behaviors similar to the experimental results in Figure 3b, which can be associated with their intrinsic asymmetric geometries that result in different interactions of the surface plasmons with left-handed and right-handed circularly polarized light. Briefly, the DNA origami plays the dominant role in determining the chiral response of the symmetric 3D AuNR dimer nanoarchitectures. In contrast, structural chirality dominates the chiroptical activity of the asymmetric nanoarchitectures. However, it remains unknown how the chiral DNA molecules quantitatively affect the observed chiroptical activity via dipole−plasmon Coulomb interaction. To fully understand the plasmonic chirality of the 3D AuNR dimers, complex theoretical models must be developed to calculate the individual contributions from plasmon−plasmon and DNA−plasmon interactions by simulating the DNA origami as a 2D molecular dipole array. Nevertheless, in this work we have successfully developed a facile strategy that can be used for rational manipulation of the plasmonic chirality through DNA-directed self-assembly of AuNRs into 3D nanoarchitectures with simple adjustments of the spatial configuration.

In conclusion, we have employed a 2D DNA origami as a bifacial scaffold to direct the assembly of 3D plasmonic nanoarchitectures by designing two batches of capturing strands on the opposite sides of the DNA origami. For the first time, anisotropic AuNRs were precisely located on both sides of the rectangular bifacial DNA origami to generate discrete 3D tunable plasmonic nanoarchitectures. The resultant unique chiral optical activities were experimentally observed and rationally tailored by modifying the 3D spatial configuration of the nanoarchitectures. Our strategy shows great potential for future plasmonic chirality studies, such as the "chiral plasmonic ruler", where shifting the location of a single AuNR in the 3D dimer nanoarchitecture at nanometer scale leads to strong perturbations of the plasmonic CD. Also, precise positioning of other optical components (e.g., quantum dots and fluorescent molecules) on the surface of the underlying DNA origami template should enable coupling to the localized surface plasmon in the assembled 3D plasmonic nanoarchitecture for various nanophotonic applications, such as radiative decay engineering and directional fluorescence emission. Furthermore, the bifacial DNA origami employed in our strategy promisingly allows for the assembly of hierarchical 3D suprastructures upon sequence-specific hybridization between the neighboring DNA origami, which will open a new door to the well-defined fabrication of complex and functional 3D nanostructures.

■ ASSOCIATED CONTENT

Ⓢ Supporting Information

Experimental details, DNA sequences, cryo-EM images, UV−vis spectra, and calculations of CD of the pure metallic AuNR nanostructures. This material is available free of charge via the Internet at http://pubs.acs.org.

■ AUTHOR INFORMATION

Corresponding Author

qbwang2008@sinano.ac.cn

Author Contributions

†X.L. and Z.C. contributed equally.

Notes

The authors declare no competing financial interest.

■ ACKNOWLEDGMENTS

Q.W. acknowledges funding by Chinese Academy of Sciences Bairen Ji Hua Program and Strategic Priority Research Program (XDA01030200), the National Natural Science Foundation of China (21073225, 91023038), the National Science Foundation of Jiangsu Province (BK2012007), the Chinese Ministry of Science and Technology (2011CB965004), and the CAS/SAFEA International Partnership Program for Creative Research Teams.

■ REFERENCES

(1) Acuna, G. P.; Möller, F. M.; Holzmeister, P.; Beater, S.; Lalkens, B.; Tinnefeld, P. *Science* **2012**, *338*, 506.
(2) Lim, D.-K.; Jeon, K.-S.; Kim, H. M.; Nam, J.-M.; Suh, Y. D. *Nat. Mater.* **2010**, *9*, 60.
(3) Kuzyk, A.; Schreiber, R.; Fan, Z.; Pardatscher, G.; Roller, E.-M.; Högele, A.; Simmel, F. C.; Govorov, A. O.; Liedl, T. *Nature* **2012**, *483*, 311.
(4) Shen, X.; Song, C.; Wang, J.; Shi, D.; Wang, Z.; Liu, N.; Ding, B. *J. Am. Chem. Soc.* **2012**, *134*, 146.
(5) Benson, O. *Nature* **2011**, *480*, 193.
(6) Bidault, S.; García de Abajo, F. J.; Polman, A. *J. Am. Chem. Soc.* **2008**, *130*, 2750.
(7) Maune, H. T.; Han, S. P.; Barish, R. D.; Bockrath, M.; Goddard, W. A., III; Rothemund, P. W. K.; Winfree, E. *Nat. Nanotechnol.* **2010**, *5*, 61.
(8) Liu, K.; Nie, Z.; Zhao, N.; Li, W.; Rubinstein, M.; Kumacheva, E. *Science* **2010**, *329*, 197.
(9) Lo, P. K.; Altvater, F.; Sleiman, H. F. *J. Am. Chem. Soc.* **2010**, *132*, 10212.
(10) Zheng, J.; Constantinou, P. E.; Micheel, C.; Alivisatos, A. P.; Kiehl, R. A.; Seeman, N. C. *Nano Lett.* **2006**, *6*, 1502.
(11) Pal, S.; Deng, Z.; Ding, B.; Yan, H.; Liu, Y. *Angew. Chem.* **2010**, *122*, 2760.
(12) Pal, S.; Deng, Z.; Liu, Y.; Yan, H. *J. Am. Chem. Soc.* **2011**, *133*, 17606.
(13) Ding, B.; Deng, Z.; Yan, H.; Cabrini, S.; Zuckermann, R.; Bokor, J. *J. Am. Chem. Soc.* **2010**, *132*, 3248.
(14) Luk'yanchuk, B.; Zheludev, N. I.; Maier, S. A.; Halas, N. J.; Nordlander, P.; Giessen, H.; Chong, C. T. *Nat. Mater.* **2010**, *9*, 707.
(15) Liu, N.; Hentschel, M.; Weiss, T.; Alivisatos, A. P.; Giessen, H. *Science* **2011**, *332*, 1407.
(16) Soukoulis, C. M.; Wegener, M. *Nat. Photonics* **2011**, *5*, 523.
(17) Auguié, B.; Alonso-Gómez, J. L.; Guerrero-Martínez, A.; Liz-Marzán, L. M. *J. Phys. Chem. Lett.* **2011**, *2*, 846.
(18) Christofi, A.; Stefanou, N.; Gantzounis, G.; Papanikolaou, N. *J. Phys. Chem. C* **2012**, *116*, 16674.
(19) Li, F.; Gao, D.; Zhai, X.; Chen, Y.; Fu, T.; Wu, D.; Zhang, Z.-P.; Zhang, X.-E.; Wang, Q. *Angew. Chem., Int. Ed.* **2011**, *50*, 4202.
(20) Zhao, Z.; Jacovetty, E. L.; Liu, Y.; Yan, H. *Angew. Chem., Int. Ed.* **2011**, *50*, 2041.
(21) Li, Z.; Zhu, Z.; Liu, W.; Zhou, Y.; Han, B.; Gao, Y.; Tang, Z. *J. Am. Chem. Soc.* **2012**, *134*, 3322.
(22) Guerrero-Martínez, A.; Auguié, B.; Alonso-Gómez, J. L.; Džolić, Z.; Gómez-Graña, S.; Žinić, M.; Cid, M. M.; Liz-Marzán, L. M. *Angew. Chem., Int. Ed.* **2011**, *50*, 5499.
(23) Ko, S. H.; Du, K.; Liddle, J. A. *Angew. Chem., Int. Ed.* **2013**, *52*, 1193.
(24) Ke, Y.; Lindsay, S.; Chang, Y.; Liu, Y.; Yan, H. *Science* **2008**, *319*, 180.
(25) Maoz, B. M.; Chaikin, Y.; Tesler, A. B.; Elli, O. B.; Fan, Z.; Govorov, A. O.; Markovich, G. *Nano Lett.* **2013**, *13*, 1203.